Computational discovery of single-layer III-V materials

Houlong L. Zhuang, Arunima K. Singh, and Richard G. Hennig*
Department of Materials Science and Engineering, Cornell University, Ithaca, New York 14853, USA
(Received 9 December 2012; revised manuscript received 19 February 2013; published 8 April 2013)

Single-layer materials open up tremendous opportunities for nanoelectronic devices. Using a first-principles design approach we identify a previously unrecognized family of single-layer III-V materials. We determine their energetic and dynamical stability, identify a surprising reconstruction, and calculate their electronic properties using a hybrid density functional and the G_0W_0 method. Finally, we find that metal substrates stabilize these as-yet hypothetical materials. Our results provide guidance for experimental synthesis efforts and future searches of single-layer materials suitable for device applications.

DOI: 10.1103/PhysRevB.87.165415 PACS number(s): 73.22.−f, 63.22.Np, 71.15.Mb, 73.61.Ey

I. INTRODUCTION

The last two decades have seen an explosion of interest in two-dimensional materials, which now can be synthesized in either single or a few atomic layer form.[1–3] The discovery of novel fabrication methods for creating two-dimensional materials such as graphene,[4] zinc oxide,[5] silicon carbide,[6] boron nitride,[7] and molybdenum disulfide[8] has opened a new field of materials research with promising applications in nanoelectronic devices. Single-layer materials not only represent the ultimate scaling in the vertical direction, but also show a variety of novel and useful electronic, optical, and mechanical properties. However, the number of materials that have been synthesized in two-dimensional (2D) form is limited. There are potentially many more candidate materials awaiting discovery, which could have transformative properties in device applications.[9,10]

Density-functional theory (DFT) has the potential to predict the stability of proposed materials and has already played an important role in predicting the existence of single-layer materials. For example, metastable structures of silicene and graphyne have been predicted by DFT,[11,12] and experimental efforts have tried synthesizing these single-layer materials.[13] Searches for other 2D materials, especially semiconductors beyond those already fabricated, have continued.[9,10]

The two primary questions in this search are (i) what is the stability of these single-layer materials and (ii) how are their electronic structures altered due to reduced dimensionality. In this paper, we answer these two questions for the family of single-layer group-III-V materials. We first identify all suitable candidate materials that exhibit the same 3D crystal structure types as occur in the systems with known 2D materials. To determine the stability of the 2D materials, we compare the formation energies to the corresponding bulk energies and calculate their phonon spectra. For 2D materials with unstable phonon modes, we investigate different reconstructions. Hybrid density-functional and G_0W_0 calculations that can accurately predict the band gap of materials[14–16] are used to determine the band structure of the 2D materials. Finally, we construct a diagram illustrating the relationship between band gaps and lattice constants which supplements current 3D materials selection diagrams that are widely used for the design of electronic devices in the semiconductor industry.

II. METHODS

All calculations are based on DFT using the projector augmented wave (PAW) method as implemented in the plane-wave code VASP.[17–19] For the structural relaxations and energy calculations we employ the generalized gradient approximation with the PBE parametrization.[20] To overcome the problem of band-gap underestimation in semilocal exchange-correlation functionals, the Heyd-Scuseria-Ernzerhof (HSE06) hybrid functional and the G_0W_0 method are used for calculating the band structures.[14–16,21] A cutoff energy of 400 eV for the plane-wave basis set is used throughout all calculations and ensures an accuracy of the energy of 1 meV/atom. The k-point sampling uses the Monkhorst-Pack scheme[22] and employs for the 2D materials a $120 \times 120 \times 1$ mesh for the PBE functional, a $12 \times 12 \times 1$ mesh for the more expensive HSE06 functional, and a $32 \times 32 \times 32$ mesh for the bulk systems resulting in a similar accuracy as the cutoff-energy convergence. For the G_0W_0 calculations, we employ 64 bands, 96 frequency points, and a $18 \times 18 \times 1$ k-point mesh. For the 2D materials a vacuum spacing of 18 Å ensures that the interactions between the layers are negligible.

We identify all materials that exhibit the same 3D crystal structure types as occur in the systems with the known 2D materials C, BN, ZnO, SiC,[4–7] using the Inorganic Crystal Structure Database.[23] For the group-III-V systems, the relevant 3D crystal structures are wurtzite and zinc blende. Initially, we assume that all binary group-III-V 2D materials have the same hexagonal structure as single-layer boron nitride and then explore buckled hexagonal and other structures.[24] We fully optimize all structures until the forces and in-plane stresses are converged to within 1 meV/Å and 0.01 GPa, respectively.

The energetic stability of the proposed single-layer materials with respect to their bulk forms is determined by the energy difference $\Delta E = E_{2D}/N_{2D} - E_{3D}/N_{3D}$, where E_{2D} and E_{3D} denotes the energy of the 2D and 3D bulk (zinc blende or wurtzite) system, respectively. N_{2D} and N_{3D} refer to the number of atoms in the respective unit cells.

To investigate the dynamical stability of all single-layer materials we calculate their phonon spectra, using density-functional perturbation theory.[25,26] Due to the heteropolar characteristics of each material, it is important to include the long-range Coulomb forces in the force-constant matrix.[25,27]

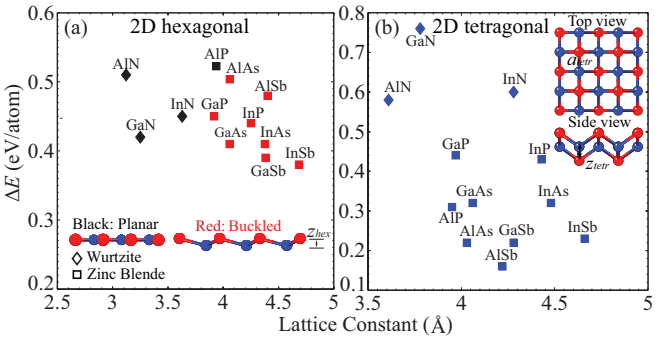

FIG. 1. (Color online) Energy differences ΔE between the 2D and bulk structures as a function of lattice parameter for 2D group-III-V materials with (a) hexagonal and (b) tetragonal structure. The diamond and square symbols denote the energy differences with respect to the hexagonal wurtzite and cubic zinc-blende structure, respectively. Black indicates that the hexagonal structure is planar, while red means that the hexagonal structure is buckled.

The force constants consist of both analytic and nonanalytic contributions, the latter of which depends on the Born effective charges Z^* and the macroscopic dielectric constant ϵ_∞.[25] We calculate Z^* and ϵ_∞ and include the nonanalytic contribution in our force-constant matrix to determine the phonon spectra.

III. RESULTS

A. Single-layer hexagonal III-V materials

Figure 1(a) and Table I show the energy differences $\Delta E_{\rm hex}$ and lattice parameters $a_{\rm hex}$ of the hexagonal 2D group-III-V materials. The formation energies relative to the respective bulk phases range from 0.38 eV/atom for InSb to 0.52 eV/atom for AlP. While these formation energies are quite high, they are comparable to that of single-layer SiC ($\Delta E_{\rm hex} = 0.50$ eV/atom), which has indeed been fabricated successfully.[6] This indicates that it might be feasible to grow hexagonal single-layer III-V materials on suitable substrates that reduce the formation energies and stabilize the structures.

Two types of hexagonal structures, a planar and a buckled one, are obtained by relaxations.[9] The buckling is illustrated in Fig. 1(a) and the amount of buckling $z_{\rm hex}$ is shown in Table I. We observe that the nitrides and AlP prefer planar structures, while all others exhibit buckled structures. This structure trend can be understood from the energy balance between (i) the electrostatic potential energy of the ions and (ii) the bonding energy of the sp^2 and sp^3 hybridization that is reflected in the preference of each ion for a trigonal planar or pyramidal configuration.

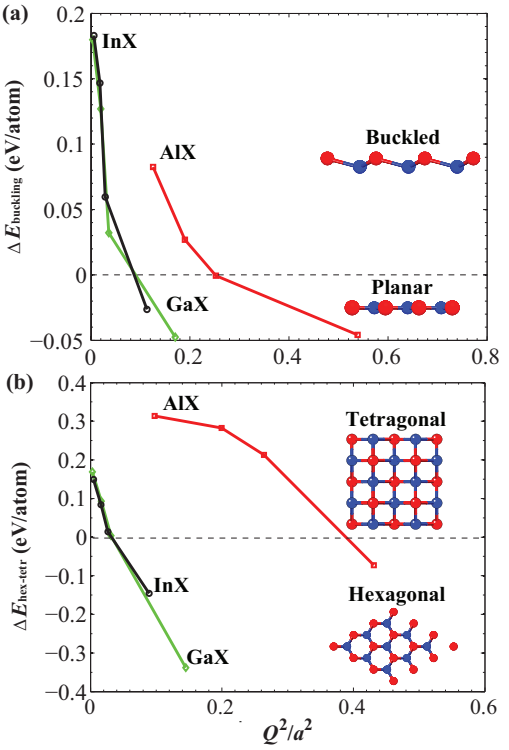

FIG. 2. (Color online) (a) Energy difference between hexagonal planar and hexagonal buckled geometries as a function of Q^2/a^2. (b) Energy difference between the hexagonal and tetragonal geometries as a function of Q^2/a^2.

The alternating buckling of the layered hexagonal materials results in a dipole moment across the layer whose electrostatic energy is proportional to Q^2/a^2, where Q is the ionic charge of the species and a is the lattice parameter. Figure 2(a) shows that for each group in the III-V family, the energy difference $\Delta E_{\rm buckling}$ between the hexagonal planar and buckled geometries decreases rapidly with increasing Q^2/a^2, illustrating the importance of the electrostatic interaction in the stabilization of the buckled and planar structures. The large electronegativity difference for the nitrides and AlP results in large ionic charges that is reflected in the Bader charges shown in Table II. The large charges combined with their small lattice parameters

TABLE I. Structural parameters and energy differences ΔE of the 2D hexagonal and tetragonal group III-V materials relative to the known 3D crystal structures. The structural parameters include the lattice constants a and the buckling displacements z.

	AlN	AlP	AlAs	AlSb	GaN	GaP	GaAs	GaSb	InN	InP	InAs	InSb
						2D hexagonal						
$\Delta E_{\rm hex}$ (eV/atom)	**0.51**	0.52	0.50	0.48	**0.42**	0.45	0.41	0.39	**0.45**	0.44	0.41	0.38
$a_{\rm hex}$ (Å)	3.12	3.94	4.06	4.40	3.25	3.91	4.06	4.38	3.63	4.25	4.38	4.68
$z_{\rm hex}$ (Å)	0	0	0.45	0.63	0	0.43	0.59	0.70	0	0.52	0.67	0.76
						2D tetragonal						
$\Delta E_{\rm tetr}$ (eV/atom)	0.58	**0.31**	**0.22**	**0.16**	0.76	**0.44**	**0.32**	**0.22**	0.60	**0.43**	**0.32**	**0.23**
$a_{\rm tetr}$ (Å)	3.61	3.95	4.03	4.22	3.78	3.97	4.06	4.28	4.28	4.43	4.48	4.66
$z_{\rm tetr}$ (Å)	0.58	1.41	1.56	1.80	0.68	1.50	1.61	1.80	0.63	1.55	1.69	1.88

TABLE II. Electronic and phonon properties of the 2D hexagonal group-III-V materials. Shown are the band gaps E_g^{HSE} and the electron and hole effective masses m_e^*/m_e and m_h^*/m_e, respectively, obtained from HSE06 calculations, the quasiparticle band gaps from G_0W_0 calculations, the Bader charges Q_{Bader} transferred from the group-III to the group-V atoms, the Born effective charges Z^*, the macroscopic dielectric constant ϵ_∞, the phonon frequencies ω_{LO} and ω_{TO} at the Γ point, and the frequency splitting $\Delta\omega$.

	AlN	AlP	AlAs	AlSb	GaN	GaP	GaAs	GaSb	InN	InP	InAs	InSb
						Electronic structure						
E_g^{HSE} (eV)	4.85	3.24	2.49	2.07	3.23	2.51	1.83	1.43	1.52	1.80	1.41	1.25
$E_g^{G_0W_0}$ (eV)	5.03	3.93	3.08	2.17	4.00	3.21	2.39	1.88	1.57	2.32	1.81	1.62
m_e^*/m_e	1.24	0.59	0.48	0.38	0.69	0.41	0.33	0.28	0.43	0.37	0.32	0.28
m_h^*/m_e	2.33	1.37	1.20	1.01	1.97	1.16	1.06	0.91	2.26	1.39	1.27	1.09
Q (e)	2.29	1.98	1.77	1.56	1.34	0.74	0.57	0.27	1.22	0.72	0.59	0.36
Z^* (e)	2.71	3.02	2.92	2.79	3.23	3.12	3.06	2.85	3.83	3.44	3.39	3.20
ϵ_∞	1.64	2.57	3.11	4.11	1.98	3.24	4.16	5.64	4.08	3.64	4.74	5.80
						Phonon properties						
ω_{LO} (cm^{-1})	903	569	434	355	809	442	302	237	647	369	332	190
ω_{TO} (cm^{-1})	812	524	403	335	722	409	282	226	592	335	306	179
$\Delta\omega$ (cm^{-1})	91	45	31	20	87	33	20	11	55	34	26	11

make the buckling energetically unfavorable in the nitrides and AlP.

The ionic interactions alone, however, are not sufficient to completely explain the observed structural trends and the preference for each of the ions in the III-V compounds for sp^2 or sp^3 hybridization needs to be considered. The group-III elements B, Al, Ga, and In can all form planar trigonal sp^2 bonded molecular structures with D_{3h} symmetry, e.g., trihydrides and trihalides. For the group-V elements, the most common configuration is pyramidal trigonal. For the case of the nitrogen atom, a trigonal planar configuration can form if the lone pair occupies a p orbital that can participate in an aromatic bond by forming π bonds. An example for such a system is indole, where the energetic stabilization from the aromatic system leads to the formation of sp^2 orbitals and a trigonal planar nitrogen configuration. The small energy difference between sp^2 and sp^3 bonded configurations of nitrogen is also reflected in the small activation energy for pyramidal inversion of trivalent nitrogen compounds such as in NH_3. In contrast, in phosphorous compounds and compounds of the heavier group-V elements, Ga and In, this activation energy is considerably greater owing to the stronger energetic preference for sp^3 hybridization. In general, the heavier group-V elements P, As, and Sb favor trigonal pyramidal sp^3 bonded configurations with C_{3v} symmetry, as seen in the trihydrides.[28]

The combination of the trend to form sp^3-bonded trigonal pyramidal structures for the heavier group-V elements and the lower electrostatic energy (Q^2/a^2) for the later group-III-V compounds explains the observation that only the nitrides and AlP exhibit planar hexagonal configurations.

The dynamical stability of the hexagonal 2D materials is determined by the phonon spectra shown in Fig. 3. Out of the 12 III-V materials only AlP, AlAs, and GaSb show imaginary frequencies, demonstrating that the other nine are dynamically stable. The phonon frequencies at high-symmetry k points agree with previous studies.[9] However, one notable difference is that our calculations capture an important phonon feature of heteropolar materials, the splitting of longitudinal and transverse optical modes (denoted as the LO and TO branches in Fig. 3) at the Γ point.

Table II shows the Born effective charges Z^*, the macroscopic dielectric constants ϵ_∞, the phonon frequencies of the LO and TO branches (ω_{LO} and ω_{TO}), as well as the splitting magnitude $\Delta\omega = \omega_{\mathrm{LO}} - \omega_{\mathrm{TO}}$ for the 2D hexagonal III-V materials. As can be seen, the frequency splitting magnitude follows the same trend as the ionicity trend in each cation subgroup. For example, in the subgroup of In pnictides, $\Delta\omega$ decreases from 55 cm^{-1} for InN to merely 11 cm^{-1} for InSb. AlN has the largest $\Delta\omega$ due to its high ionicity.

Table II also lists the Bader charges Q that describe how much charge is transferred from the group-III to the group-V atoms in the 2D hexagonal structures. We find that the charge transfer decreases in each subgroup following electronegativity trends. As a consequence of the decreased ionicity, the structures buckle and the orbital hybridization changes from sp^2 to sp^3. Noteworthy, while a static description of the charge, the Bader charge follows the frequency splitting trend in each subgroup, namely, a larger Bader charge transfer corresponds to a larger LO-TO splitting magnitude.

B. Single-layer tetragonal III-V materials

The phonon spectra of hexagonal AlP, AlAs, and GaSb shown in Fig. 3 indicate that they are dynamically unstable. A possible reason for the instability is the dipole moment in the direction perpendicular to the single-layer plane. Thus, a reconstruction that reduces the dipole moment could stabilize the structure. We start with a planar hexagonal configuration and displace neighboring cation-anion pairs perpendicular to the plane such that the net dipole moment is zero. Optimization of this structure results in a tetragonal structure illustrated in the insets of Fig. 1(b). This structure has space group 129 ($P4/nmm$), Schönflies symbol D_{4h}^7, and is characterized by the lattice constant a_{tetr} and the out-of-plane displacement z_{tetr}. Surprisingly, unlike the threefold coordinated planar or buckled hexagonal structure, each cation and anion in the tetragonal structure is bonded to four neighboring anions and cations, respectively. The 2D tetragonal AlP, AlAs, and GaSb structures are mechanically stable as illustrated by their phonon spectra in Fig. 3.

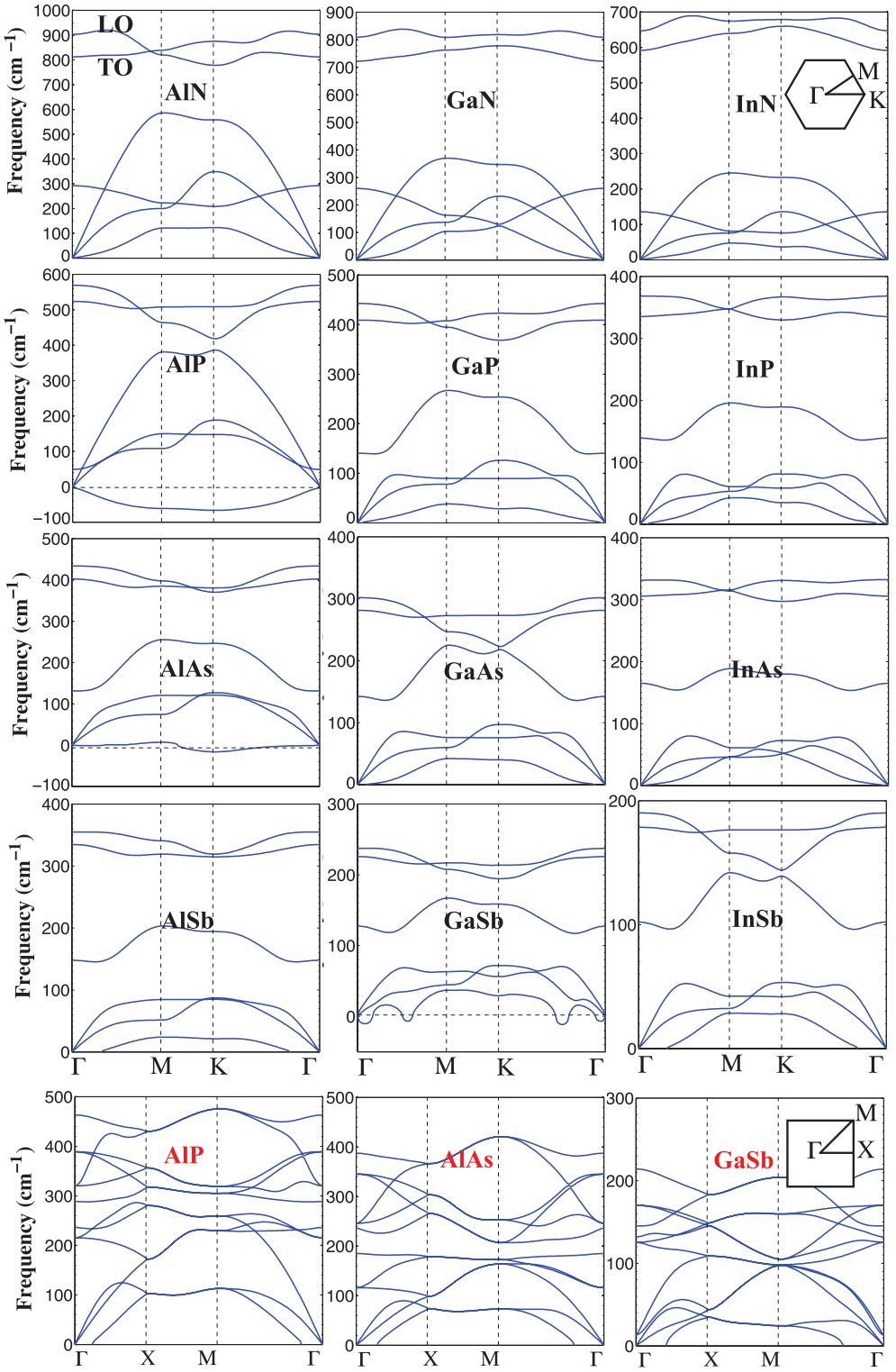

FIG. 3. (Color online) Phonon spectra of hexagonal (black labels) and tetragonal (red labels) 2D group-III-V materials. The insets show the sketches of the first Brillouin zones of the 2D hexagonal and tetragonal structures.

To further test the stability of the tetragonal 2D materials, we perform *ab-initio* molecular dynamics simulations for the tetragonal AlP system using a $5 \times 5 \times 1$ supercell and the PBE functional. A Nosé thermostat sets the temperature to 600 K.[29] The simulation is performed for a total time of 2 ps using a time step of 1.5 fs. Geometry optimizations of several molecular dynamics snapshots for the tetragonal AlP system result in the original tetragonal structure. This suggests that 2D tetragonal AlP is stable at a temperature of 600 K.

Although most of the III-V materials are dynamically stable in the 2D hexagonal structure, we also calculate their energy in the tetragonal structures. Table I and Fig. 1(b) show their

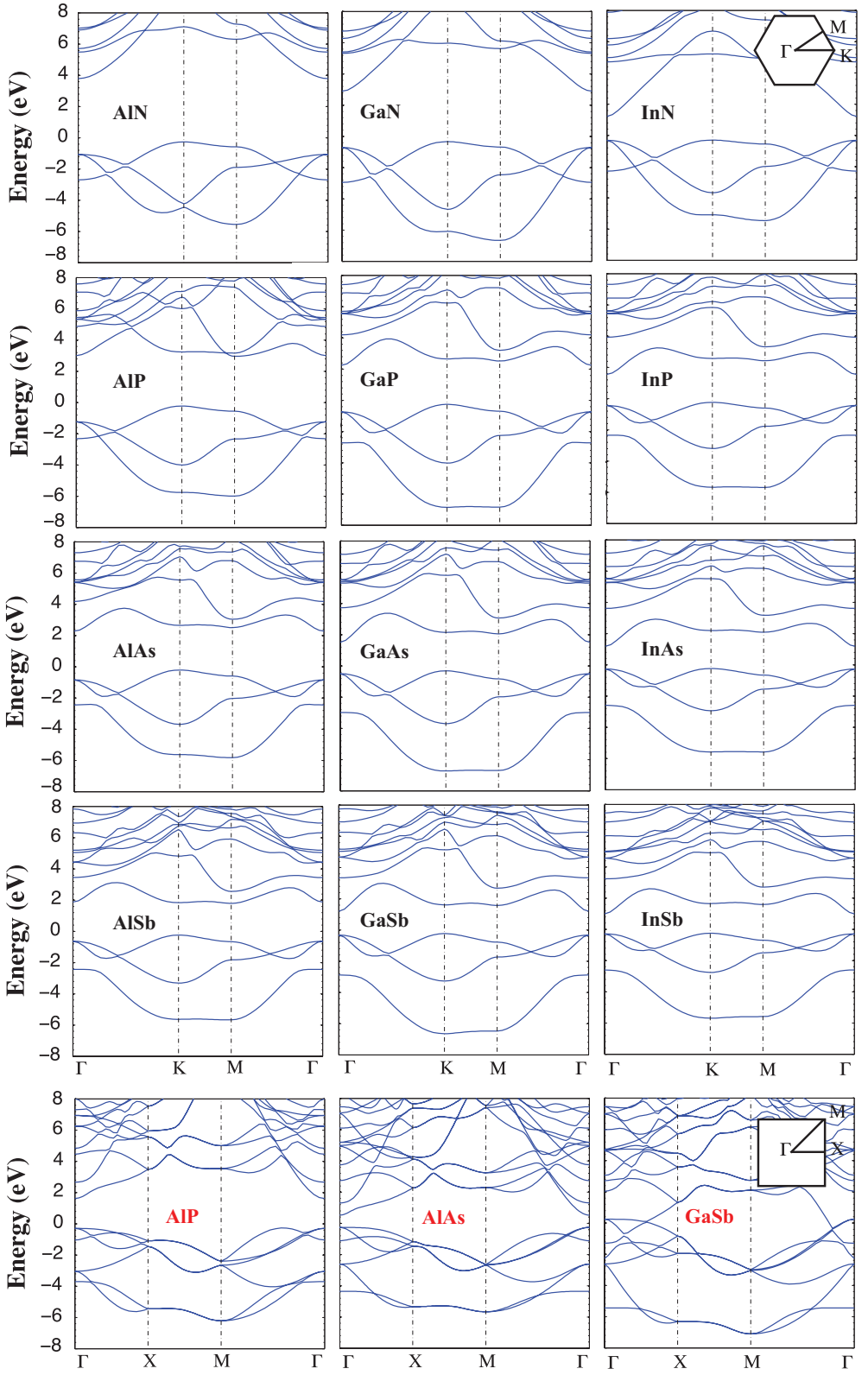

FIG. 4. (Color online) Band structures of hexagonal (black labels) and tetragonal (red labels) 2D group-III-V materials calculated with the HSE06 hybrid functional.

energy relative to the bulk phases and the structural parameters. Except for AlN, GaN, and InN, all other III-V materials have lower energies in the tetragonal structure than the hexagonal one. Therefore, the hexagonal structure is not the only possible metastable 2D structure for the group-III-V materials. The energy ΔE_{tetr} decreases in each subgroup. Notably, some 2D

tetragonal III-V materials have very low formation energies of the order of 0.2 eV/atom. For example, the formation energy of AlSb is 0.16 eV/atom which is close to the energy of the previously synthesized ZnO of 0.19 eV/atom. This indicates that it is more likely to grow AlSb in the 2D tetragonal structure than in the 2D hexagonal one.

To understand why tetragonal structures are favored over hexagonal structures in most group-III-V materials, we plot the energy difference $\Delta E_{\text{hex}-\text{tetr}}$ between the hexagonal and tetragonal structures as a function of Q^2/a^2 of the hexagonal structures in Fig. 2(b). The energy difference $\Delta E_{\text{hex}-\text{tetr}}$ decreases with increasing importance of the electrostatic interactions measured by Q^2/a^2. This trend is consistent with the explanation that most 2D group-III-V materials tend to form tetragonal structures in order to reduce their dipole moment perpendicular to the layered materials.

C. Electronic structure of single-layer III-V materials

Figure 4 shows the band structures obtained using the HSE06 hybrid functional and Table II compares the band gaps obtained with the HSE06 functional and the G_0W_0 method. The HSE06 and the G_0W_0 method predict similar band gaps with the G_0W_0 band gaps being slightly larger. Comparison with experimental data for the single-layer materials BN, fluorographene, and MoS_2 show that the GW method in these related systems overestimates the band gap.[9,30] As expected, all the band structures of the 2D hexagonal structures exhibit similar shapes. One common feature of these band structures is the occurrence of the valence-band maximum (VBM) at the K point, whereas the conduction-band minimum (CBM) positions appear at the Γ point. In other words, all these hexagonal 2D materials have indirect band gaps, different from the corresponding 3D group-III-V materials with mixed band-gap types.[31] For example, InP has a direct band gap in three dimensions, and the band-gap type changes to indirect due to dimension reduction.

Figure 5 shows the relationship between the size of the band gap of the 2D materials and their lattice constants. As illustrated by the color spectrum, most of the band gaps lie within the range of visible light, indicating that these 2D materials may be useful for optoelectronic or photocatalytic applications. Of all 12 materials, AlN has the largest band gap of 4.85 eV. However, this value is still small compared to its wurtzite bulk phase, which has a wide band gap of 6.2 eV.[33]

An important parameter for semiconductor device materials is the electron/hole effective mass, denoted as m_h^* and m_e^*, respectively. These parameters affect carrier mobility. From the HSE06 band structure we calculate the average m_e^* for the CBM at the Γ point, and the m_h^* for the VBM at the K point. Table II lists the effective masses $m_{e/h}^*$ of the 2D hexagonal materials. The relative $m_{e/h}^*$ are illustrated in Fig. 5. The m_e^* of most hexagonal 2D group-III-V materials are comparable to silicon, which has an average $m_e^* = 0.26m_e$.[34] In addition, these m_e^* are similar to or smaller than that of single-layer MoS_2 with a theoretical value of $m_e^*/m_e = 0.483$.[32] Single-layer MoS_2 has recently been shown to work in transistor devices.[35] The similarity between the calculated electronic properties illustrates the potential of the predicted 2D hexagonal III-V materials for electronics applications.

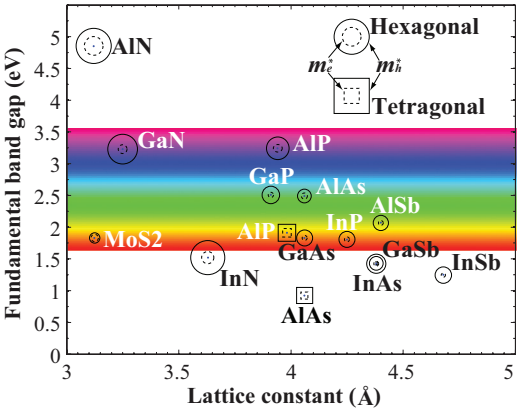

FIG. 5. (Color online) The relationship between fundamental band gaps and lattice constants of the semiconducting 2D group-III-V materials. A sketch of the light spectrum is overlaid to aid visualization of the band-gap size. The center of the two concentric circles or squares determines the band-gap size of hexagonal and tetragonal structures, respectively. Additionally, the inner and outer radii or side lengths represent the electron and hole effective mass, respectively. The data of single-layer MoS_2 are shown for comparison.[32]

With the HSE06 functional, we also calculate the band structures of the 2D tetragonal structures exhibiting lower energies than their hexagonal counterparts. Surprisingly, except AlP and AlAs, the other seven materials become metallic. The band structures of AlP, AlAs, and GaSb are shown in Fig. 4. It can be seen that even the band-gap types of AlP and AlAs are different. AlP has an indirect band gap of 1.89 eV, while AlAs has a direct band gap of 0.79 eV. Moreover, the m_e^* of tetragonal AlP and AlAs at the Γ point are 0.50 and 0.40 m_e, respectively.

To understand the origin of the metallic character of most tetragonal 2D materials, we analyze the density of states for 2D hexagonal and tetragonal GaSb shown in Fig. 6. For the semiconducting hexagonal GaSb, Fig. 6(a) shows that the valence-band maximum is dominated by the Sb p states. The conduction-band minimum (CBM) on the other

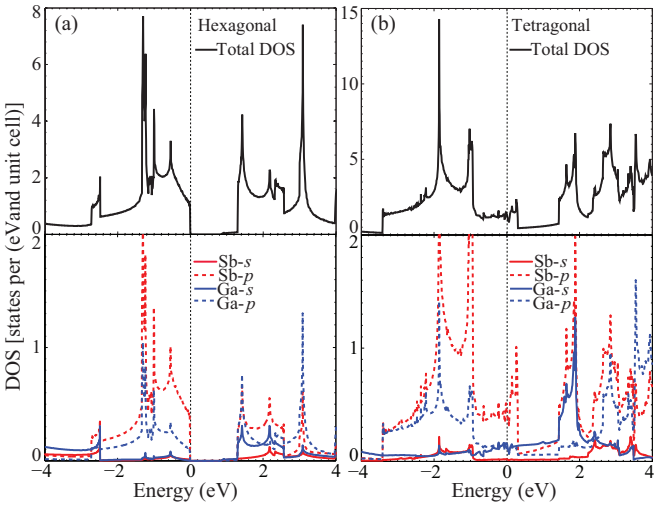

FIG. 6. (Color online) Total density of states (DOS) and projected DOS of (a) hexagonal and (b) tetragonal GaSb.

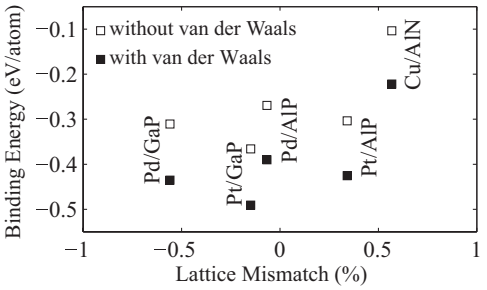

FIG. 7. Adsorption energy of 2D tetragonal III-V materials on (100) surfaces of common metal substrates, Cu, Pd, and Pt with lattice mismatches less than 1%. The filled and empty squares denote adsorption energies with and without the inclusion of van der Waals interactions, respectively. The substrates significantly enhance the stability of the 2D materials.

hand is dominated by about equal contributions from the Sb s and Ga sp^3 states. In contrast, for metallic tetragonal GaSb, Fig. 6(b) shows that the density of states near the Fermi level is dominated by the p states of Sb with the sp^3 states of Ga being absent. The metallic character of the 2D tetragonal GaSb originates from the partly filled band that is dominated by states of p character localized on the Sb sites. Although the semiconductor-to-metal transition may be less appealing for growing 2D semiconductors, stacking various tetragonal structures may lead to useful metal-semiconductor heterojunctions.

D. Substrate stabilization of single-layer III-V materials

High quality, uniform and large domains of graphene have been grown on metal substrates.[36,37] The metal surfaces efficiently catalyze the chemical vapor deposition process and stabilize graphene. Similarly, to synthesize the 2D III-V materials predicted in this work, suitable substrates are required that reduce the formation energies and stabilize the structures. Since most of the 2D tetragonal III-V materials have already quite low formation energies, we search the Inorganic Crystal Structure Database[23] for suitable lattice-matched substrate materials and calculate the adsorption energies.

We identify five combinations of (100) surfaces of commonly used metal substrates, namely Cu, Pt, and Pd, and 2D tetragonal III-V materials that exhibit lattice mismatches of less than 1%. We calculate the adsorption energies for these five combinations by modeling the transition metal surfaces as slabs consisting of eight layers. The atoms in the bottom three layers are fixed to their bulk positions. The 2D materials are strained appropriately to match the lattices of the substrates. Our calculations reproduce the experimental interlayer spacing contraction between the surface layers of (100) Cu of $d_{12} = 2.0 \pm 0.5\%$.[38] The binding energy E_b is calculated as

$$E_b = \frac{E_{2D+S} - E_S - E_{2D}}{N_{2D}}, \quad (1)$$

where E_{2D+S} is the energy of the strained 2D III-V material adsorbed on the (100) surface of the substrate, E_S is the energy of the substrate slab, E_{2D} is the energy of the unstrained 2D III-V materials, and N_{2D} is the number of atoms in the 2D material's cell, which is 4 in this case.

Figure 7 shows the adsorption energies of the 2D tetragonal materials on these lattice-matched common metal substrates. The III-V materials are chemisorbed on the metal surfaces, unlike graphene which is weakly physisorbed on transition metal substrates.[39–41] This is due to the polar nature of the III-V materials. The substrates significantly reduce the formation energies of the 2D materials. For example for 2D tetragonal AlP on Pd, the adsorption energy of 0.27 eV/atom reduces the formation energy from 0.31 eV/atom to a mere 40 meV/atom, comparable to the formation energy of free-standing films of graphene or BN.[10]

van der Waals interactions between the tetragonal 2D materials and substrates, modeled using a vdW-DF functional with the optB88 exchange functional,[42] further increase the adsorption energy to 0.39 eV/atom, effectively reducing the energy of 2D tetragonal AlP below that of the 3D bulk phase. A similar enhancement of the adsorption energy is expected for combinations of other metal substrates and 2D III-V materials. This demonstrates that these hypothetical 2D materials could be synthesized on lattice-matched substrates.

IV. CONCLUSIONS

In summary, we identified a large number of metastable 2D materials in the group-III-V family. We identified three different 2D structures that are dynamically stable in this family of materials: a planar honeycomb hexagonal structure, a buckled hexagonal structure, and a surprising low-energy tetragonal structure. Using the HSE06 functional, we obtained accurate energy band gaps and electron/hole effective masses. Calculations for potential substrates show that these 2D materials can be stabilized. Our results provide valuable guidance to synthesis efforts and potential applications of 2D group-III-V materials.

ACKNOWLEDGMENTS

We thank M. Spencer and R. Hoffmann for fruitful discussions. This work was supported by the NSF through the Cornell Center for Materials Research under Award No. DMR-1120296 and in part by the CAREER award No. DMR-1056587. This research used computational resources of the Texas Advanced Computing Center under Contract No. TG-DMR050028N and of the Computation Center for Nanotechnology Innovation at Rensselaer Polytechnic Institute.

*rhennig@cornell.edu

[1] P. W. Sutter, J.-I. Flege, and E. A. Sutter, Nat. Mater. **7**, 406 (2008).

[2] C. L. Freeman, F. Claeyssens, N. L. Allan, and J. H. Harding, Phys. Rev. Lett. **96**, 066102 (2006).

[3]D. Wu, M. G. Lagally, and F. Liu, Phys. Rev. Lett. **107**, 236101 (2011).
[4]K. S. Novoselov, A. K. Geim, S. V. Morozov, D. Jiang, Y. Zhang, S. V. Dubonos, I. V. Grigorieva, and A. A. Firsov, Science **306**, 666 (2004).
[5]C. Tusche, H. L. Meyerheim, and J. Kirschner, Phys. Rev. Lett. **99**, 026102 (2007).
[6]S. S. Lin, J. Phys. Chem. C **116**, 3951 (2012).
[7]C. Jin, F. Lin, K. Suenaga, and S. Iijima, Phys. Rev. Lett. **102**, 195505 (2009).
[8]K. F. Mak, C. Lee, J. Hone, J. Shan, and T. F. Heinz, Phys. Rev. Lett. **105**, 136805 (2010).
[9]H. Şahin, S. Cahangirov, M. Topsakal, E. Bekaroglu, E. Akturk, R. T. Senger, and S. Ciraci, Phys. Rev. B **80**, 155453 (2009).
[10]H. L. Zhuang and R. G. Hennig, Appl. Phys. Lett. **101**, 153109 (2012).
[11]S. Cahangirov, M. Topsakal, E. Aktürk, H. Şahin, and S. Ciraci, Phys. Rev. Lett. **102**, 236804 (2009).
[12]D. Malko, C. Neiss, F. Viñes, and A. Görling, Phys. Rev. Lett. **108**, 086804 (2012).
[13]P. Vogt, P. De Padova, C. Quaresima, J. Avila, E. Frantzeskakis, M. C. Asensio, A. Resta, B. Ealet, and G. Le Lay, Phys. Rev. Lett. **108**, 155501 (2012).
[14]J. Heyd, J. E. Peralta, G. E. Scuseria, and R. L. Martin, J. Chem. Phys. **123**, 174101 (2005).
[15]L. Hedin, Phys. Rev. **139**, A796 (1965).
[16]W. G. Aulbur, L. Jönsson, and J. W. Wilkins, Solid State Phys. **54**, 1 (1999).
[17]G. Kresse and J. Furthmüller, Phys. Rev. B **54**, 11169 (1996).
[18]P. E. Blöchl, Phys. Rev. B **50**, 17953 (1994).
[19]G. Kresse and D. Joubert, Phys. Rev. B **59**, 1758 (1999).
[20]J. P. Perdew, K. Burke, and M. Ernzerhof, Phys. Rev. Lett. **77**, 3865 (1996).
[21]J. Heyd, G. E. Scuseria, and M. Ernzerhof, J. Chem. Phys. **118**, 8207 (2003).
[22]H. J. Monkhorst and J. D. Pack, Phys. Rev. B **13**, 5188 (1976).
[23]G. Bergerhoff and I. D. Brown, *Crystallographic Databases* (International Union of Crystallography, Chester, 1987).
[24]N. Alem, R. Erni, C. Kisielowski, M. D. Rossell, W. Gannett, and A. Zettl, Phys. Rev. B **80**, 155425 (2009).
[25]S. Baroni, S. de Gironcoli, A. Dal Corso, and P. Giannozzi, Rev. Mod. Phys. **73**, 515 (2001).
[26]M. Gajdoš, K. Hummer, G. Kresse, J. Furthmüller, and F. Bechstedt, Phys. Rev. B **73**, 045112 (2006).
[27]G. Grosso and G. P. Parravicini, *Solid State Physics* (Academic, San Diego, 2000).
[28]E. V. Anslyn and D. A. Dougherty, *Modern Physical Organic Chemistry* (University Science Books, Sausalito, California, 2006).
[29]S. Nosé, J. Chem. Phys. **81**, 511 (1984).
[30]C. Ataca and S. Ciraci, J. Phys. Chem. C **115**, 13303 (2011).
[31]O. Madelung, *Semiconductors: Data Handbook* (Springer, New York, 2004).
[32]W. S. Yun, S. W. Han, S. C. Hong, I. G. Kim, and J. D. Lee, Phys. Rev. B **85**, 033305 (2012).
[33]H. Yamashita, K. Fukui, S. Misawa, and S. Yoshida, J. Appl. Phys. **50**, 896 (1979).
[34]R. N. Dexter, B. Lax, A. F. Kip, and G. Dresselhaus, Phys. Rev. **96**, 222 (1954).
[35]B. Radisavljevic, A. Radenovic, J. Brivio, V. Giacometti, and A. Kis, Nat. Nanotechnol. **6**, 147 (2011).
[36]K. S. Novoselov, V. I. Falko, L. Colombo, P. R. Gellert, M. G. Schwab, and K. Kim, Nature (London) **490**, 192 (2012).
[37]C. Soldano, A. Mahmood, and E. Dujardin, Carbon **48**, 2127 (2010).
[38]D. S. Sholl and J. A. Steckel, *Density Functional Theory a Practical Introduction* (Wiley, New York, 2009).
[39]G. Giovannetti, P. A. Khomyakov, G. Brocks, V. M. Karpan, J. van den Brink, and P. J. Kelly, Phys. Rev. Lett. **101**, 026803 (2008).
[40]M. Fuentes-Cabrera, M. I. Baskes, A. V. Melechko, and M. L. Simpson, Phys. Rev. B **77**, 035405 (2008).
[41]M. Vanin, J. J. Mortensen, A. K. Kelkkanen, J. M. Garcia-Lastra, K. S. Thygesen, and K. W. Jacobsen, Phys. Rev. B **81**, 081408 (2010).
[42]J. Klimeš, D. R. Bowler, and A. Michaelides, Phys. Rev. B **83**, 195131 (2011).